

FOULING OF STEAM GENERATOR TUBES IN NUCLEAR POWER PLANTS: LABORATORY TESTS TO REPRODUCE OXIDES DEPOSITION

C. Goujon^{1,2}, T. Pauporté², C. Mansour¹, S. Delaunay¹ and J-L. Bretelle³

¹ EDF R&D/Chemistry and Corrosion Group, Avenue des Renardieres, 77818 Moret-sur-Loing Cedex, France,
christophe.goujon@edf.fr, carine.mansour@edf.fr

²LECIME – UMR7575, CNRS–ENSCP, 11 rue Pierre et Marie Curie, 75231 Paris Cedex 05, France

³EDF Power Generation Division, 1 Place Pleyel, 93200 Saint Denis, France

ABSTRACT

In the secondary circuit of nuclear Pressurized Water Reactors (PWR), magnetite (Fe_3O_4) deposits lead to Steam Generator (SG) fouling. After relatively long term operation, this phenomenon causes the decrease of thermal performances and may enhance risks of the SG tube cracking. As a counteraction, chemical cleanings have become the priority strategy to remove oxide deposits in the SGs of the EDF power plant fleet. To investigate their impact on SG tubes surface reactivity, a three steps R&D program was established: (i) reproduce deposits on SG tube surfaces, (ii) apply chemical cleanings and (iii) study the redeposition of magnetite. An electrochemical study was performed to settle an experimental protocol to deposit magnetite on Inconel 600 substrates. Magnetite films with a thickness up to several dozens of micrometers were grown by cathodic electrodeposition from an alkaline Fe(III)-Triethanolamine electrolytic solution. The electrochemical potential range of magnetite deposition was identified by coupling voltamperometric and chronoamperometric studies.

INTRODUCTION

Corrosion products generated in the steam, feedwater and condensate systems of the secondary circuit of PWRs are transferred by the water flow from the feedwater to the steam generator (SG). Corrosion products deposition leads to SG fouling. They can be deposited in a loose form or as agglomerate in a partially rock-hard layer, and are non-uniformly distributed. These deposits not only reduce the efficiency of the SG by deterioration of the heat transfer, but may also cause an acceleration of the corrosion of SG tubes and blockage of support plates (Green et al., 1995). The careful selection of materials and optimization of the chemistry management of the secondary circuit fluid can limit the corrosion and the fouling of SG but are not sufficient (Alves-Vieira et al., 2010). Moreover, accumulated hard sludge cannot be efficiently removed by mechanical methods such as sludge lancing (Hur et al.,

2003). That is why chemical cleanings, started in 1989, have become since 2006 the priority strategy to remove oxides deposit in SGs of the EDF (Electricité De France) fleet. Five chemical cleanings processes are used by EDF to restore heat transfer reliability and availability of SGs. Among these processes, two are called curative cleanings, using hard physical and chemical conditions in order to recover the nominal safety operating conditions of the SGs and three are called preventive cleanings, using softer conditions in order to prevent the consequences of excessive fouling and tube support plate blockage.

Although the chemical nature of the deposits depends on the nature of materials used in the secondary circuit, it mainly consists of magnetite (80 %) (Pujet, 2002). The use of chelating agents in chemical cleaning processes may affect the passive layer of SG tubes, made of a nickel base alloy (Inconel 600 TT and 690 TT), and then may modify their surface reactivity. To investigate this impact, a three steps R&D program was established at EDF: (i) reproduce deposits on SG tube surfaces using several techniques, (ii) apply chemical cleanings and (iii) study the redeposition of magnetite in specific experimental loops.

Magnetite is a ferromagnetic material with an inverse spinel structure. Due to its magnetic and electrical properties (Cornell and Schwertmann, 2003), magnetite is often studied for application such as magnetic memory, magnetoreceptors, etc... (Teja et al., 2009; Miyamoto et al., 1994). One method to produce magnetite films is electrodeposition by oxidation of Fe(II) (Abe et al., 1983; Sorenson et al., 2002) or reduction of Fe(III) (Kothari et al., 2006; Mitra et al., 2006) at the electrode surface, followed by a chemical reaction. Inspired by the hydrothermal method developed by Sapiezko and Matijevic to produce magnetite powder from Fe(III)-Triethanolamine (TEA) solution using reducing agent (Sapiezko et al., 1980), the Switzer research group has developed a method to produce magnetite films by cathodic deposition (Kothari et al., 2006; Kulp et al. 2009) on gold and stainless steel substrates.

In the present paper, we develop a method to form adherent magnetite films with a thickness up to several dozens of micrometers by cathodic electrodeposition from

an alkaline Fe(III)-TEA electrolytic solution. The aim of this study is to settle an experimental protocol to deposit magnetite on nickel base alloys, Inconel 600 and 690. These specimens simulate fouled substrates which will be introduced in the chemical cleaning experimental loop in the next step of the study. Therefore, magnetite deposits need to be adherent in order to prevent their removal by a simple convective movement of a solution at their surface in the loop. Also, magnetite films need to be homogeneous with very well known characteristics because they constitute a reference for the deposits formed after chemical cleanings.

EXPERIMENTAL SECTION

Films deposition

The magnetite layers were deposited on two types of substrates: Inconel 600 TT and 690 TT with dimensions 20x10x2 mm. The substrates were mechanically polished (grain size 320, 600 then 1200), carefully cleaned with soap, rinsed with deionized water prior to be sonicated 5 min in acetone and 5 min in ethanol. A thin layer of commercial varnish was applied to prevent the formation of deposit on the substrate back side. The electrochemical deposition was carried out in a three-electrode cell. The reference electrode was a saturated calomel electrode (SCE) (with potential at +0.25 V/NHE) placed in a separate compartment maintained at room temperature. The counter-electrode was a platinum wire. To ensure a deposition as homogeneous as possible, the substrate was fixed in front of the counter electrode and a magnetic stirrer ensured the solution homogenization. The deposition medium was prepared with MilliQ quality water (18.2 MΩ cm). It was prepared by dissolving 1.3 g of Fe(III) sulfate hydrate in 7.5 mL of 1 M TEA, resulting in a deep red colored solution. This solution was diluted with 25 mL of water. It was then added to a second solution of 6.0 g of NaOH in 42.5 mL of water at 80°C. The resulting solution was gray-green colored with pH 12.5 at 25°C. After deposition, the deposit was rinsed with deionized water then dry in air.

Film characterizations

Film thicknesses were measured with a Dektak 6M stylus profiler. An adhesive strip was stuck on the substrate before performing the deposition. At the end of the deposit, the strip was removed in order to measure the thickness of the deposit with the profilometer. Sample morphologies were examined with a high resolution Sigma Zeiss scanning electron microscope (SEM) at an acceleration voltage of 10 kV. The X-ray analysis of each film was performed using a X'Pert PANalytical diffractometer with Cu-Kα radiation ($\lambda = 1.5406 \text{ \AA}$). Iron concentration measurements were performed using a Thermofisher ICAP 6500 ICP-AES apparatus. Mass uptake study was performed using a quartz coated by a gold electrode with a 1.37 cm² surface area and a QCM200 Stanford Research Systems microbalance.

RESULTS

Electrochemical study

Electrochemical studies using cyclic voltammetry have shown that the reduction of Fe(III)-TEA complexes is a one electron process in which an Fe(III)-TEA complex is reduced to an Fe(II)-TEA complex (Mohr et al., 2001; Bechtold et al., 2005). This reaction, which may occur as expressed in Eq. (1), is driven applying a negative potential at the working electrode which is the substrate. The Fe(III)-TEA complex then chemically reacts with the Fe(II)-TEA to produce magnetite (Eq. (2)) at the surface of the substrate. Equation (3) is the overall electrochemical reaction leading to the formation of magnetite deposit on the substrate.

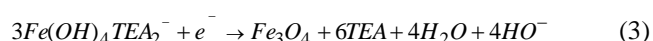
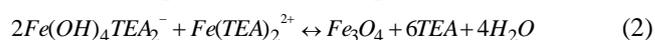


Figure 1 shows linear sweep voltammograms on an Inconel 600 TT substrate in a blank solution, i.e an alkaline TEA bath (dotted line), and the deposition bath (solid line) at 80°C. From their open circuit potentials to -1.40 V/SCE, they are swept at 5 mV/s. The voltammogram of blank solution shows that alkaline TEA is electrochemically inactive and that hydrogen evolution begins around -1.1 V/SCE. The electrochemical reduction of Fe(III)-TEA is observed at potential more negative than -1.00 V/SCE. The first reduction wave of this linear sweep, observed between -1.00 and -1.20 V/SCE, characterized a one electron reaction corresponding to Eq. (1). Between -1,20 and -1,30 V/SCE, a two-electron process occurred with the reduction of Fe(II) to Fe then for more negative potential the increase of the cathodic current density was due to hydrogen gas evolution. At the end of the first wave (-1.20 V/SCE), the current density was about -19 mA/cm² whereas it was about -63 mA/cm² for the second wave at -1.30 V/SCE. By subtracting current densities due to hydrogen generation at these potentials (-4 mA/cm² at -1.20 V/SCE; -12 mA/cm² at -1.30 V/SCE) current density of the second wave was about three times more important than the one of the first reduction wave. This observation is consistent with a one-electron reaction between -1.00 and -1.20 V/SCE and a two-electron reaction at more negative potentials.

Figure 2, focused on the first reduction wave of the voltammogram. It shows the presence of a slope change around -1.11 V/SCE, which may correspond to the deposition of two different species on the substrate. Indeed, the surface concentration of Fe(III) depends on the departure from equilibrium. At low overpotentials, the Fe(III) surface concentration is nearly the same as the bulk concentration, whereas at high overpotentials, the surface concentration of Fe(III) approaches zero. As a result, magnetite films grown at low overpotentials could be nonstoichiometric and rich in Fe(III). Whereas at high overpotentials films could be rich in Fe(II) and lead to the

formation of another iron oxide. Voltammograms reproduced under the same conditions on Inconel 690 TT substrates led to the same observations (not shown). In the following, only results from the study on Inconel 600 TT will be presented knowing that the experiments performed on Inconel 690 TT led to the same results.

Potentiostatic layer depositions and film characterizations

To confirm observations from voltammograms and identify the species deposited on the different ranges of potential, layers were deposited at constant applied potential and stopped after a constant -3 C/cm^2 charge exchanged. They were characterized by XRD analysis and SEM observations.

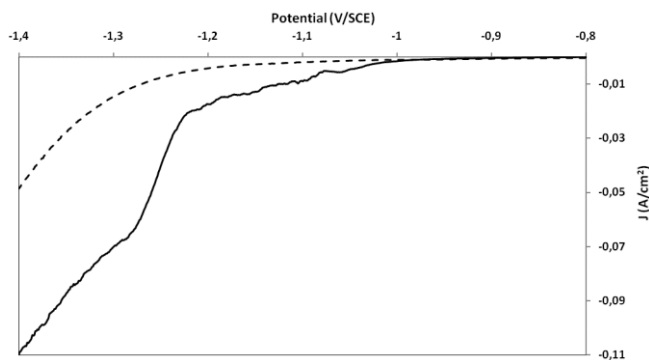


Fig. 1 Linear sweep voltammograms of alkaline-TEA solution (dotted line) and Fe(III)-TEA solution (solid line) at 80°C scanned at 5 mV/s on an Inconel 600 TT substrate.

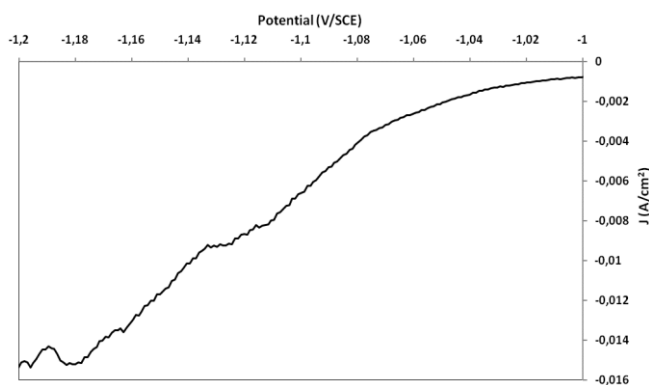


Fig. 2 Linear sweep voltammograms of Fe(III)-TEA solution at 80°C scanned at 5 mV/s on an Inconel 600 TT substrate.

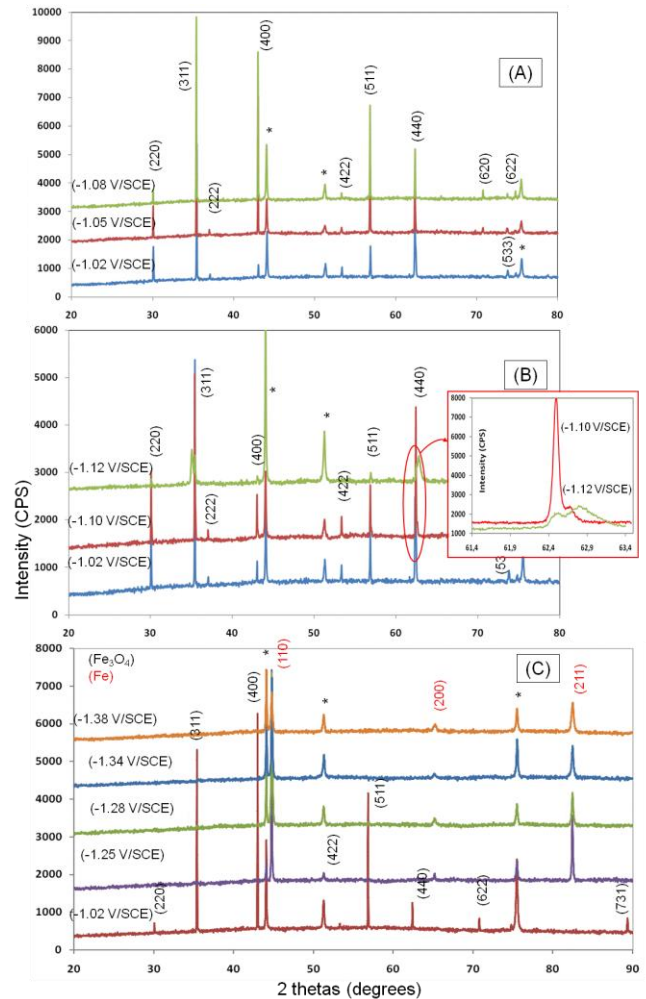


Fig. 3 XRD patterns of films deposited on Inconel 600 TT in the potentials ranges $[-1.00; -1.09 \text{ V/SCE}]$ (A), $[-1.10; -1.20 \text{ V/SCE}]$ (B), and $[-1.20; -1.40 \text{ V/SCE}]$ (C).

Adherent black films were deposited in the potential range $[-1.01; -1.09 \text{ V/SCE}]$. Between -1.10 and -1.20 V/SCE , the as-electrodeposited films were green colored prior to become intense black with a reddish tinge once dried in air. In this range, films deposited at potentials more negative than -1.14 V/SCE were not adherent once dried whereas films deposited at higher potential presented two adherent layers. When the potential became more negative ($< -1.20 \text{ V/SCE}$), gray films were produced. The X-ray diffraction patterns (Fig. 3) allowed us to identify the film material deposited at the different potentials. Films deposited between -1.00 and -1.09 V/SCE (Fig. 3A) are made of magnetite (JCPDS 19-629, lattice parameter $a=8.3980 \text{ \AA}$). XRD patterns (Fig. 3) shows that magnetite films deposited in this potential range have no preferred orientation and the lattice parameter presents a slow decrease as the deposition potential becomes more negative ($a=8.408 \text{ \AA}$ at -1.02 V/SCE and $a=8.384 \text{ \AA}$ at -1.09 V/SCE). In the $[-1.10; -1.20 \text{ V/SCE}]$ potential range, XRD patterns show a split of (311) and (440) peaks and a broadening of (511) peak (Fig. 3B). The split of (311) and (440) peaks may be attributed to the deposit of ferrihydrite as it can be

indexed as (100) and (110) reflections of this compound (JCPDS 01-072-7673). This observation is consistent with the study of Kulp et al. (Kulp et al., 2009), which reported the presence of ferrihydrite by Mössbauer Spectroscopy on films deposited on HOPG (Highly Ordered Pyrolytic Graphite) in the same electrochemical system. However, we can note that the two lattice parameters calculated from the diffraction peaks at 62.84° observed for the sample deposited at -1.12 V/ECS could also be indexed by the maghemite (440) diffraction (JCPDS 39-1346, $a=8.3515$ Å). Films deposited at potentials more negative than -1.20 V/SCE (Fig. 3C) presented XRD patterns consistent with body centered cubic iron with a lattice parameter $a=2.8598$ Å (JCPDS 01-087-0721, $a=2.8662$ Å).

The film morphologies investigated by SEM (Fig. 4) are consistent with the XRD characterizations. In the $[-1.01; -1.09$ V/SCE] potential range, as shown in the SEM image of a film deposited at -1.05 V/SCE (figure 4A), magnetite formed at rather low overpotentials had highly faceted and dense morphologies. This morphology is homogeneous on the whole surface of the deposit. In figure 4B, films deposited at -1.08 V/SCE had a dense globular morphology with no well-defined crystal morphology. Films deposited in the potential range $[-1.10; -1.20$ V/SCE] had filament-like microstructures, as seen in Fig. 4C. Image of the section of the deposit (Fig. 4C, inset) at -1.11 V/SCE suggests the presence of two layers which is consistent with the first observations of the deposit. Iron films grown at potential more negative $[-1.20; -1.40$ V/SCE] had a dense well-covering morphology with rather large crystallites (Fig. 4D).

This first part of the study enabled us to confirm the observations made on the voltammograms. In order to settle a protocol to control magnetite films growing on Inconel 600 TT and 690 TT substrates, the potential range of interest is $[-1.00; -1.10$ V/SCE].

Protocol optimization

Deposit current (faradaic) efficiency η , based on the profilometer measurements of film thicknesses, were calculated over the $[-1.00; -1.12$ V/SCE] potential range with the Eq. (4). Profilometer measurements at these potentials revealed the homogeneity of the surface morphology and thickness which allowed us to perform this calculation from Eq. (5) and Eq. (6).

$$\eta = \frac{mass_{measured}}{mass_{theory}} \quad (4)$$

$$mass_{measured} = S_{deposit} * h_{deposit} * \rho_{Fe_3O_4} \quad (5)$$

$$mass_{theory} = \frac{Q}{n * F} * M_{Fe_3O_4} \quad (6)$$

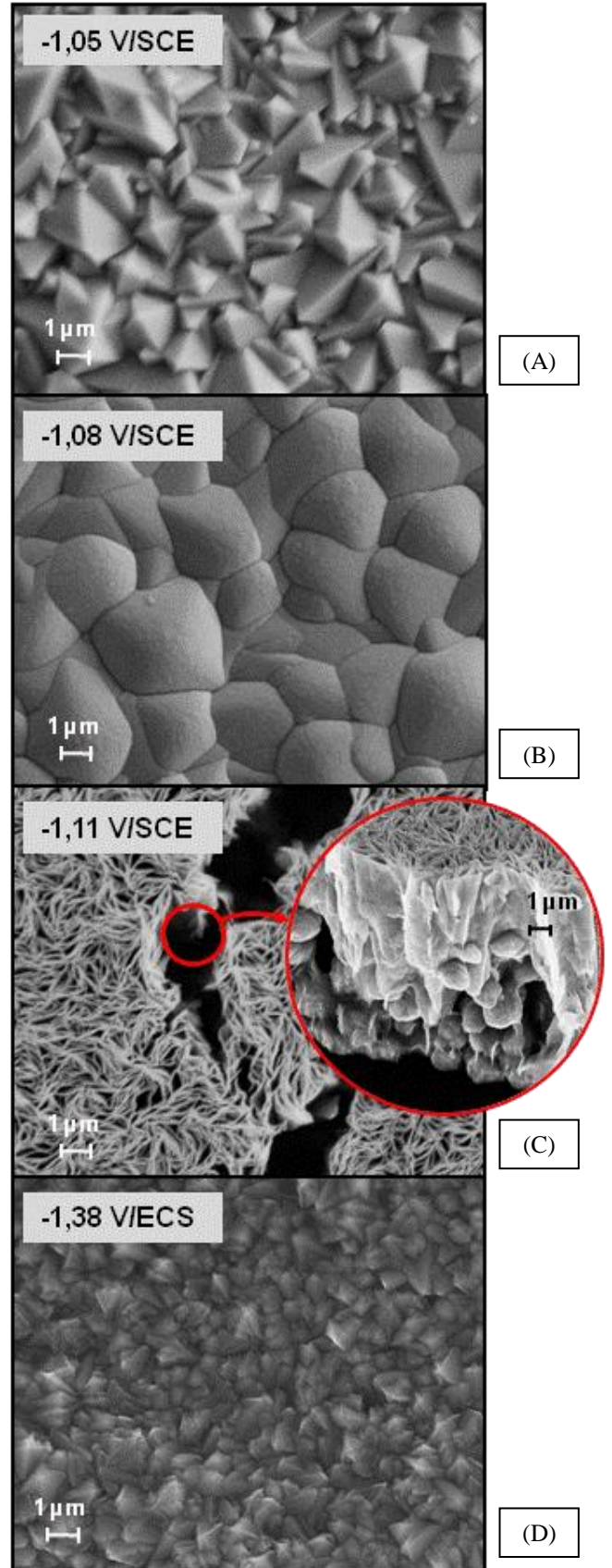


Fig. 4 SEM images of films deposited on Inconel 600 TT at 80°C at -1.05 (A), -1.08 (B), -1.12 (C), -1.38 (D) V/SCE.

Results presented in Fig. 5A show a small increase of deposit current efficiency between -1.02 and -1.05 V/SCE then it is nearly constant until -1.10 V/SCE. Although ferrihydrite deposition is suspected at lower potential, deposit current efficiencies were calculated based on the same model and showed an increase to reach 73 % at -1.12 V/SCE. To confirm this tendency, the experiment was repeated on the same potential range then each deposit was dissolved in 10 mL of HCl 32 % during 5 minutes. Iron concentration of each dissolved deposit was measured by ICP-AES. Figure 5B presents the comparison between the quantity of iron calculated and measured after oxide dissolution. Iron quantity was calculated based on the thickness of films supposing that deposits were formed with pure magnetite (Fig. 5B, cross line) in [-1.00; -1.12 V/SCE] potential range and pure ferrihydrite (Fig. 5B, diamond line) in [-1.10; -1.12 V/SCE] potential range. ICP-AES analysis (Fig. 5B, square line) showed a decrease of iron concentration at potentials more negative than -1.09 V/SCE. This tendency is opposed to the one with pure magnetite deposit calculations which confirms the synthesis of another iron oxide, supposed to be ferrihydrite, at these potentials.

To back-up these results, additional experiments were performed on a gold coated quartz substrate of a microbalance for a constant charge of -0.3 C/cm^2 . Prior to these depositions, voltamograms performed on microbalance showed a similar electrochemical behavior compared to Inconel 600 TT electrodes but with lower cathodic current densities on gold substrate. Therefore it could be considered as a qualitative analogue of the Inconel 600 TT electrochemical system. Masses deposited on microbalance at several potentials are presented in Fig. 5C. Results show the increase of mass deposited between -1.00 and -1.05 V/SCE, then it is nearly constant until -1.10 V/SCE confirming the previous observations on the deposit current efficiency. Then masses deposited on gold substrate slowly decreased as potentials became more negative and collapsed for potential more negative than -1.18 V/SCE. This sharp decrease is probably due to the increase of hydrogen generation at the gold substrate which prevents iron adherence at the surface of the substrate and negatively affect the mass measurement. In order to grow magnetite films with the best current efficiency, the choice of potential should be done close to the upper limit of the potential range [-1.00; -1.09 V/SCE]. As current efficiency increase is negligible on [-1.05; -1.09 V/SCE] and the SEM images shows that deposits at potential more negative than -1.07 V/SCE are probably nonstoichiometric, -1.05 V/SCE appeared to be the best compromise to grow pure magnetite films on Inconel 600 TT and 690 TT.

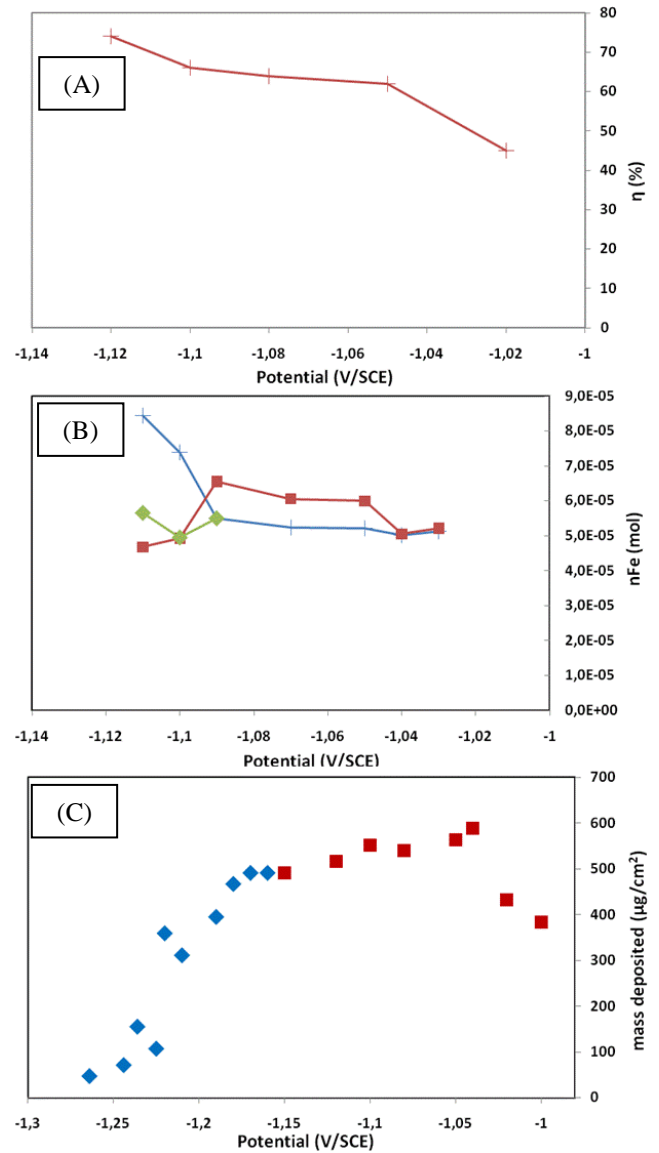


Fig. 5 Electrodeposition faradaic efficiency of deposits on Inconel 600 TT at 80°C (A). Iron quantity of material deposited based on magnetite (cross) and ferrihydrite (diamond) model calculation and ICP-AES (square) measurements (B). Mass deposited on microbalance (C). Squares and diamonds refer to two different experiments.

Deposits on SGs tubes can exceed dozens of micrometers thickness. To be representative of SGs fouling, electrochemical magnetite deposit protocol should allow the formation of high thickness deposits without losing the homogeneity and purity. In order to increase deposit thickness, deposits were performed at -1.05 V/SCE for a long period. Results presented in Fig. 6, show a near linear increase of the thickness and a linear decrease of current efficiencies with the deposition time. After 7000 seconds, the deposit thickness was higher than 50 μm . Profilometer measurements and SEM observations (Fig. 6) show that grains formed by magnetite crystallites agglomerates begin to grow for films deposit higher than 30 μm .

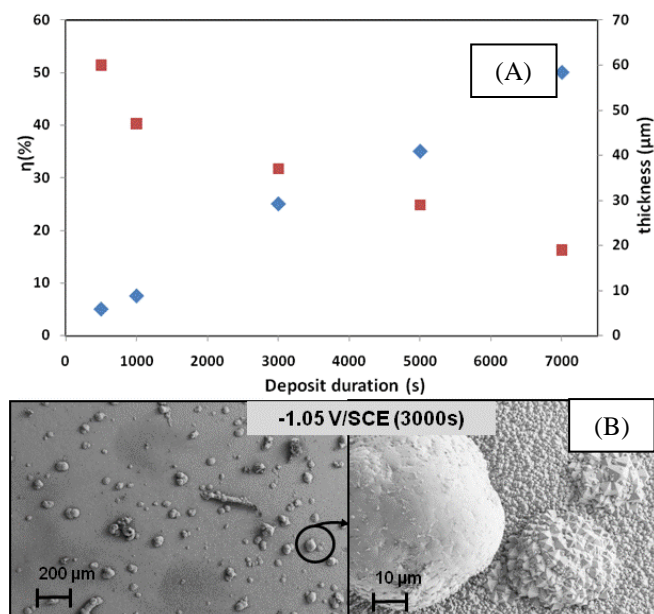


Fig. 6 (A) Current efficiency (square) and thickness (diamond) of long duration deposit at -1.05 V/SCE on Inconel 600 TT. (B) SEM images of 3000 s deposit.

Grows of these grains is coupled to the loss of the surface flatness. For all durations, XRD patterns confirmed the deposit of pure magnetite films. As the increase of magnetite is nearly linear with time deposit, the fine control of the thickness of magnetite films deposited at -1.05 V/SCE is very easy.

In order to optimize the protocol of magnetite deposition, influence of temperature and agitation were studied. Surface current densities increased with temperatures on the voltammograms which lead us to increase the temperature to get faster deposits. For instance, at -1,05 V/SCE, surface current density increase from -2,42 mA/cm^2 at 70°C to -6.86 mA/cm^2 at 90°C. However, we observed in different cases a degradation of the deposit solution with the time. This degradation, probably due to the degradation of TEA-Fe(III) complex (Yilmaz et al., 2001), occurred faster at high temperature. Therefore, the temperature was set at 80°C in study described above.

Finally influence of agitation was studied performing deposits at -1.05 V/SCE at several stirrer spin speeds. The deposition current density increased as the agitation became more intense from -1.5 mA/cm^2 without any agitation to -6 mA/cm^2 at 850 rotations/min (rpm). However, no large variation of the deposit current efficiency was observed. SEM images (Fig. 7), XRD patterns and the oxide lattice parameter were the same for all values of agitation and magnetite films had no preferred orientation. These results confirm that the influence of agitation was negligible. However, the small decrease of deposition current efficiency at faster agitation could be explained by a small influence of the convective movement of the fluid at the surface of the deposit which prevented the deposition of magnetite formed at the surface. Therefore, the agitation was set at 170 rpm in the protocol used above.

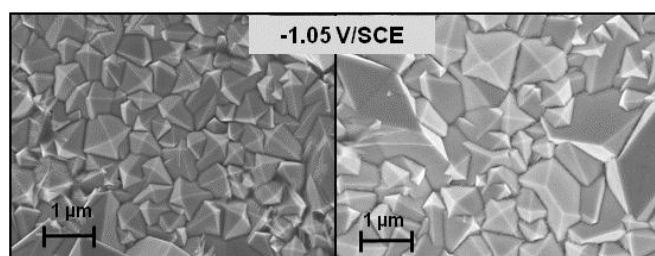


Fig. 7 SEM images of magnetite films deposited on Inconel 600TT at -1.05 V/SCE at 0 rpm (left) and 850 rpm (right).

DISCUSSION

XRD analysis, SEM observations and deposition current efficiency study of deposits performed in the [-1.10; -1.20 V/SCE] potential range show clearly the synthesis of a compound different from magnetite, and XRD results suggest that poorly crystallized ferrihydrite is the most likely formed compound. Only peak broadenings were reported by Kulp et al. (Kulp et al., 2009) whereas we observed two distinct peaks in the XRD patterns presented in figure 3B. We can also note that, (511) peak broadening may correspond to maghemite, $\gamma\text{-Fe}_2\text{O}_3$ (JCPDS 39-1346, $a=8.3515 \text{ \AA}$). In all cases, such splittings or broadenings were not observed for films deposited at -1.05 V/SCE confirming the absence of Ferrihydrite at this potential. Identification of magnetite and maghemite by XRD could appear intricate, because both phases possess the same spinel structure and close lattice parameters (Kim et al., 2012). Therefore, in order to make sure that films deposited at -1.05 V/SCE are made of pure magnetite, the ability of the XRD apparatus to distinguish diffraction peaks from maghemite and magnetite was checked. XRD measurements were conducted on commercial magnetite powder and synthesized maghemite powder using the same acquisition parameters as for the films deposited on Inconel 600 TT. Superposition of XRD patterns of the two powders presented a clear shift of (511) and (440) peaks that demonstrates the ability of the technique to discriminate the two phases. In addition, refined XRD measurements were performed around (511) peak angle for films deposited at -1.05 and -1.12 V/SCE. Whereas splitting of this peak appeared at -1.12 V/SCE, it did not show off at -1.05 V/SCE confirming the synthesis of pure magnetite at this potential. Although doubt could exist on the nature of deposit at lower potential, the describe deposition protocol at -1.05 V/SCE, insures unambiguously the synthesis of pure magnetite films which was the expected goal of this study. Characteristics of oxide deposits inside steam generators could be very different depending on the area of interest and are not well known. They are mainly formed by magnetite (80%), zinc oxide (around 7%) and silica oxide (around 7%). Depending on the nature of materials used in the secondary circuit, copper could also be present (up to 20 %) in deposits [Varin et al., 1996]. Due to complex mechanisms

of their formation, oxide deposits are usually composed of several layers on SG tubes with various characteristics (porosity, roughness). Working on electrodeposit with controlled and well known characteristics allow us to highlight more easily the impact of chemical cleanings in the next step of the study.

CONCLUSIONS

Characterization of films deposited by reduction at the Inconel 600 TT and 690 TT electrodes from a Fe(III)-TEA bath enabled to settle a protocol to grow magnetite films. Voltametry and chronoamperometry studies results were coupled to determine potentials ranges of deposit: magnetite is deposited between -1.01 and -1.09 V/SCE, ferrihydrite/magnetite films are deposited from -1.10 to -1.20 V/SCE then iron is deposited at more negative potentials. Although film identifications are not perfectly sure in the [-1.10; -1.20 V/SCE] potential range, deposits performed at -1.05 V/SCE have clearly been identified as pure magnetite. Optimization of temperature and agitation conditions allowed to settle the best efficient protocol to perform deposition of magnetite films matching our needs for the next steps of the study. Finally, pure adherent homogeneous magnetite films with a controlled thickness up to several dozens of micrometers have been deposited at -1.05 V/SCE, at 80°C with a stirring speed of 170 rpm.

The next steps of this industrial study will consist in introducing the elaborated magnetite layers in a specific experimental loop at EDF R&D and test the effects of the main SGs chemical cleanings processes on them.

NOMENCLATURE

η	current (faradaic) efficiency, %
F	Faraday constant, C/mol
Q	quantity of electric charge, C
S	deposit surface, m ²
h	deposit thickness, m
ρ	mass density, g/cm ³
M	molar mass, g/mol
rpm	rotation per minute, min ⁻¹

REFERENCES

Abe, M., Tamaura, Y., 1983, Ferrite plating in aqueous solution: a new method to prepare magnetic thin films, *J. Appl. Phys.*, Vol.22, L511-L513.

Alves-Vieira, M., Dijoux, M., de Bouvier, O., Mayos, M., Coquio, N., 2010, Impact of preventive and curative remedies for steam generators fouling and tube support plate blockage on secondary circuit materials, *Fontevraud 7 International Symposium*.

Bechtold, T., Turcanu, A., 2005, Determination of reaction rate between cathodically formed Fe(II)-TEA-complex and Fe(III)-hepta-D-gluconate complex by cyclic voltammetry, *J. Electroanal. Chem.*, Vol. 580, pp. 173-178.

Cornell, R. M., Schwertmann, U., 2003, The iron oxides: Structures, properties, occurrences and uses. *Wiley VCH*.

Green, S. J., Hetsroni, G., 1995, PWR Steam Generator, *Int. J. Multiphase Flow*, Vol. 21, pp. 1-97.

Hur, D., Choi, M., Lee, E., and Kim, U., 2003, Copper dissolution and electrochemical behaviour in EDTA-an EDA-based solutions for steam generator chemical cleaning, *Nuclear Engineering and Design*, Vol. 224, pp. 207-212.

Kim, W., Suh, C-Y., Cho, S-W., Roh, K-M., Kwon, H., Song, K., Shon, I-J., 2012, A new method for the identification and quantification of magnetite-maghemite mixture using conventional X-ray diffraction technique, *Talanta*, Vol. 94, pp. 348-352.

Kothari, H. M., Kulp, E. A., Limmer, S. J., Poizot, P., Bohannan, E. W., Switzer, J. A., 2006, Electrochemical deposition and characterization of Fe₃O₄ films produced by the reduction of Fe(III)-TEA, *J. Mater. Res.*, Vol. 21, pp. 293-301.

Kulp, E. A., Kothari, H. M., Limmer, S. J., Yang, J., Gudavarthy, R. V., Bohannan, E. W., Switzer, J. A., 2009, Electrodeposition of Epitaxial Magnetite Films and Ferrihydrite Nanoribbons on Single-Crystal Gold, *Chem. Mater.*, Vol. 21, pp. 5022-5031.

Mitra, S., Poizot, P., Finke, A., Tarascon, J.-M., 2006, Growth and Electrochemical Characterization versus Lithium of Fe₃O₄ Electrodes Made via Electrodeposition, *Adv. Funct. Mater.*, Vol. 16, pp. 2281-2287.

Miyamoto, Y., Ishihara, S., Hirano, T., Takada, M., Suzuki, N., 1994, Ferroelectricity of magnetite (Fe₃O₄) observed by means of magnetoelectric effect, *Solid State Commun.*, Vol. 89, pp. 51-54.

Mohr, S., Bechtold, T., 2001, Electrochemical behavior of iron-complexes in presence of competitive ligands: A strategy for optimization of current density, *J. Appl. Electrochem.*, Vol. 31, pp. 363-368.

Pujet, S., 2002, "Encrassement secondaire des GV : Analyse du REX et des essais en laboratoire sur le laboratoire et le depot de produits de corrosion", Rapport EDF R&D HI-84/02/008.

Sapieszko, R. S., Matijevic, E. J., 1980, Preparation of Well-Defined Colloidal Particles by Thermal Decomposition of Metal Chelates, *Colloid Interface Sci.*, Vol. 74, pp. 405-422.

Sorenson, T. A., Morton, S. A., Waddill, D. G., Switzer, J. A., 2002, Epitaxial Electrodeposition of Fe₃O₄ Thin Films on the Low-Index Planes of Gold, *J. Am. Chem. Soc.*, Vol. 124, pp. 7604-7609.

Teja, A. S., Koh, P-Y., 2009, Synthesis, properties, and applications of magnetic iron oxide nanoparticles, *Progress in Crystal Growth and Characterization of Materials*, Vol. 55, pp. 22-45.

Varin, R., 1996, characterization of PWR Steam Generators deposits, *EPRI Report TR-1060048*.

Yilmaz, V. T., Topcu, Y., Karadag, A., 2002, thermal decomposition TEA and monoethanoethylenediamine complexes of some transition metal saccharinates, *Thermochimica Acta*, Vol. 383, pp. 129-135.